Measurement of the dielectric constant of amorphous CN_x films in the 0–45 eV energy range

Francesco Barreca, Angela Maria Mezzasalma, Guglielmo Mondio,* and Fortunato Neri
Dipartimento di Fisica della Materia e Tecnologie Fisiche Avanzate
and Istituto Nazionale per la Fisica della Materia, Salita Sperone 31, I-98166, Messina, Italy

Sebastiano Trusso and Cirino Vasi
Istituto di Tecniche Spettroscopiche del CNR, Via La Farina 237, I-98123, Messina, Italy
(Received 31 May 2000)

Amorphous a-CN_x thin films were deposited at room temperature by pulsed laser ablation of graphite targets in a controlled nitrogen atmosphere. By means of reflection electron-energy-loss spectroscopy their dielectric function has been obtained in the 0–45 eV energy range. An appropriate method of analysis has been also proposed which does not take into account surface contributions to the measured spectra in the presence of large electron inelastic mean free paths. The overall results show that the nitrogen introduction in the amorphous carbon matrix induces an increase in the total threefold coordination, i.e., a progressive material graphitization. This finding is also confirmed from x-ray photoelectron spectroscopy results for the N and C 1s core levels.

I. INTRODUCTION

In the last few years carbon nitride materials have been the focus of considerable experimental and theoretical attention since Cohen and co-workers proposed that β-C_3N_4 should have a hardness comparable to that of diamond.[1,2] Subsequent calculations have shown that other crystalline C_3N_4 structures should have stability comparable to or greater than that of β-C_3N_4, and that many of these structures should be very hard (e.g., the cubic one). The only exception is represented by the energetically most stable form, the rhombohedral C_3N_4, which has a graphitelike structure and is expected to be quite soft.[3,4] From the experimental point of view carbon nitride has been observed to exist in apparent amorphous or disordered phases although there are several reports of crystalline phases being dispersed in the amorphous matrix.[5–7] The interest in amorphous carbon nitride (a-CN_x) stems from its outstanding mechanical, optical, and electronic properties, which can be tailored as a function of the nitrogen content x. Due to its strong chemical bonding it shows a marked stability that allows a large variety of applications in the fields of optical and electronic engineering, in particular with respect to the high-temperature and high-frequency applications.

The atomic structure of amorphous carbon nitride is still very poorly known. This is mainly due to the rich variety of possible local environments and the lack of long-range order. The investigations have shown competition between the C-C, C-N, and N-N bonds in forming such a structure. Even if some group claimed the growth of the β-C_3N_4 on the basis of x-ray and electron diffraction or TEM data, most of the films, prepared with several different deposition techniques, were obtained in the a-CN_x form.[8] The knowledge of the physical properties of a-CN_x as a function of both the nitrogen content and the particular deposition technique adopted, is then of great relevance. Optical properties are a useful index of changes directly related to the structure and composition of the films. They have been studied by conventional spectroscopy (near normal incidence reflectivity and ellipsometry) but only in the photon low-energy range ($E < 5$ eV).[9–14]

In this study we present the dielectric function of a-CN_x films, deposited by means of pulsed laser ablation, as deduced from reflection electron-energy-loss measurements (REELS) in the range 0–45 eV. Electron-energy-loss spectrocopy (EELS) is sensitive to the local coordination of CN structure and can be useful to evaluate and to distinguish, as a function of the nitrogen content, among various local carbon environments (i.e., threefold and fourfold coordination). EELS data of a-CN_x have been already presented in the literature[10,14–19] but only in the form of raw experimental data: neither elastic peak subtraction nor some background removal procedure have been carried out. With the aid of a proper numerical procedure the dielectric function, the bulk loss function and the reflection coefficient can be obtained over an energy range wider than that allowed by optical spectroscopy techniques. The analysis of the data from energy-loss spectra and from x-ray photoelectron spectroscopy has allowed the characterization of the overall nitrogen content in the films and the nature of the bonding states of both carbon and nitrogen.

II. EXPERIMENT

The films were grown at room temperature by ablating high purity graphite targets placed on a rotating holder, 40 mm far from the substrates. These latter were crystalline silicon and Corning 7059 glass. Ablation of the target was performed by focusing the beam of a KrF excimer laser (wavelength 248 nm, pulse width 25 ns, pulse energy 150 mJ, repetition rate 10 Hz) onto an area estimated approximately 4 mm^2 resulting in an energy density of 3.7 $J\,cm^{-2}$. The high vacuum deposition chamber was evacuated down to about 4.0×10^{-4} Pa. The samples were obtained by inserting N_2 gas with partial pressures P_{N_2} up to 13 Pa.

REELS and x-ray photoelectron spectroscopy (XPS) mea-

TABLE I. C 1*s* and N 1*s* XPS data analysis results for samples grown at different partial nitrogen pressure (see text).

	C 1*s*		N 1*s*		
x	Pos. (eV)	FWHM (eV)	N-C (sp^3)	N-C (sp^2)	FWHM (eV)
0.0	284.5	1.59			
10.4	284.8	1.85	398.7	400.1	2.1
25.0	285.1	2.07	398.8	400.5	2.1

surements were carried out using a VG ESCALAB vacuum system. Reflection electron-energy-loss spectra were obtained by a VG LEG61 electron gun in conjunction with a VG CLAM 100 hemispherical analyzer. The primary electron energy was $E_p = 2.5$ keV, the incidence angle α was about 40° from the normal to the sample surface. The gun current was about 10 μA and the pass energy of the analyzer was set to 20 eV. The acceptance angle β of the analyzer was about 3°. Under these conditions the overall energy resolution, as determined from the elastic peak [full width at half maximum (FWHM)] of the REEL spectrum was approximately 1.4 eV. The same analyzer, with the same pass energy, was used to measure x-ray photoelectron spectra excited by the Al $K\alpha$ radiation (1486.6 eV) of a conventional twin-anode Al/Mg $K\alpha$ source. During each measurement the vacuum in the analysis chamber was in the 10^{-7} Pa range. The REELS and XPS spectra were obtained by an automatic computer-controlled data acquisition system and a minimum of five complete scans were acquired in order to optimize the signal-to-noise ratio. In order to avoid charging effects, a silver paint droplet has been deposited onto a small region of the sample surface. All the measured XPS core levels were referred to the Ag $3d_{5/2}$ line (380.0 eV). A negligible amount of oxygen contamination, presumably due to atmospheric exposure of samples, was also observed. Optical reflectivity measurements were performed on both a Lambda19 and a Lambda20 Perkin-Elmer UV-VIS-NIR spectrophotometers using a specular reflectance accessory.

III. RESULTS AND DISCUSSION

XPS spectroscopy has been extensively used to characterize the composition and the chemical bonding nature of the C-N compounds.[8] We investigated the C 1*s* and N 1*s* core-level photoemission spectra to estimate both the $x = [N]/[C]$ atomic ratio and to study the modifications induced by progressive nitrogen incorporation (see Table I). In Figs. 1 and 2 such spectra are reported, after the subtraction of a Shirley-type background, for some CN_x films deposited at different nitrogen partial pressures. A quantitative estimate of the composition was performed in terms of the relative intensity of the respective 1s photoemission signals and the sensitivity factors.[20] Values of *x* up to 0.25 were determined. The effect of nitrogen incorporation on the C 1s peak is an asymmetric broadening and shifting towards higher binding energies. For the non-nitrogenated sample the C 1*s* peak is sharper (FWHM = 1.6 eV) and is located at 284.5 eV, substantially at the same value of other pure carbon systems, while it reaches 285.1 eV with FWHM = 2.1 for the highest

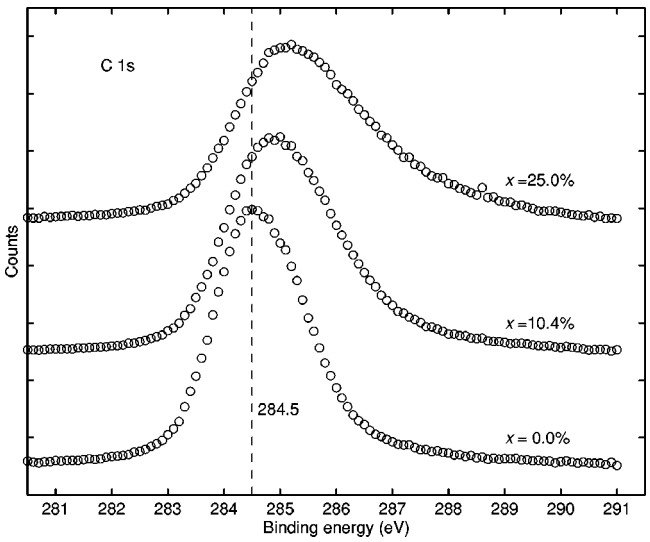

FIG. 1. Experimental C 1*s* XPS spectra of CN_x films having different nitrogen content (see Table I).

nitrogen content sample. As nitrogen is incorporated, the presence of new components is therefore evident. Nevertheless, as pointed out by other authors,[8,21] it is not possible to unambiguously deconvolve such a structure due to the many overlapping components. We rather preferred to carry out this analysis on the N 1*s* photoemission band, whose behavior is reported in Fig. 2. Extending from 398 to 401 eV, it can be very well fitted with just two components, located approximately around 398.5 and 400 eV. Since different nitrogen species give N 1*s* binding energies in this range, the assignment of these components to definite chemical states is not unique. Nevertheless, considering two main configurations for nitrogen, there is a wide agreement in the literature[8,22–25] to assign the peaks at lower and higher energy to nitrogen atoms bonded with fourfold- and threefold-coordinated carbon atoms, respectively. Overall, the low-energy peak exhibits a slight, but definite, increase with increasing nitrogen content.

The experimentally measured REEL spectra for the studied *a*-CN_x films are shown in Fig. 3, after a normalization to

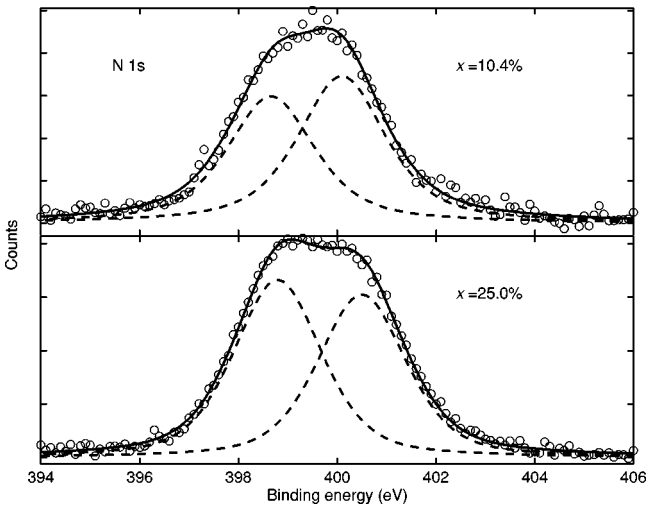

FIG. 2. Experimental and numerically fitted N 1*s* XPS spectra of CN_x films having different nitrogen content (see Table I).

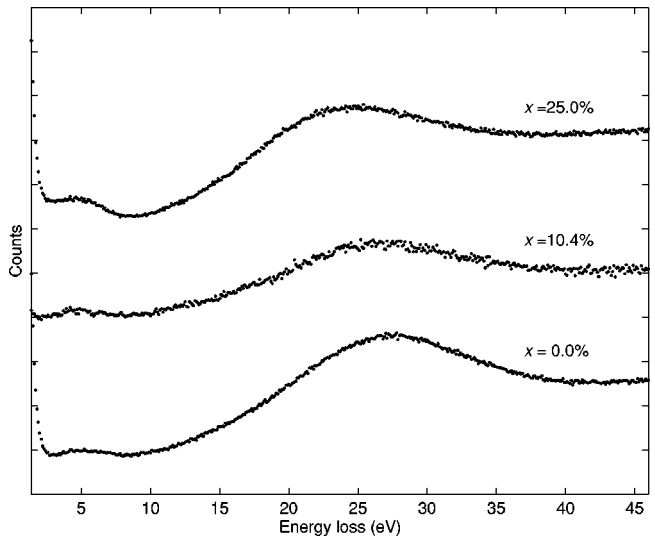

FIG. 3. Experimental energy loss spectra of CN_x films having different nitrogen content (see Table I). The curves have been shifted and the elastic peak region excluded for sake of clarity.

the intensity of the primary electrons peaks. The analysis of the spectra have been carried out on the basis of a simple phenomenological model in which the measured single scattering electron yield is represented by a linear combination of the bulk and surface loss functions. The details of the model, reported in the Appendix, show that the background-free experimental spectra are essentially due to bulk scattering, i.e., directly proportional to $\mathrm{Im}(-1/\tilde{\epsilon})$. The spectra, reported in Fig. 4, are characterized by two broad plasmon features due to collective excitations of π electrons (at lower energy) and $\pi+\sigma$ electrons (at higher energy). The dependence of $\pi+\sigma$ excitations upon the nitrogen content can be clearly seen. Their plasmon energy decreases about 2.9 eV when x varies from 0 to 0.25, ranging from 26.9 eV for the pure carbon to 24.0 eV in the case of the maximum nitrogen concentration. All the relevant parameters deduced from the analysis outlined in the preceding section are reported in Table II.

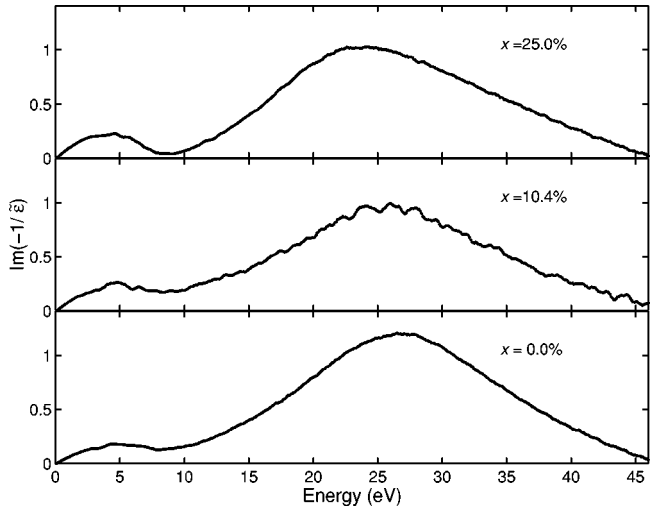

FIG. 4. $\mathrm{Im}(-1/\tilde{\epsilon})$ spectra for CN_x films having different nitrogen content (see Table I), as deduced from the procedure outlined in the Appendix.

TABLE II. Summary of parameters deduced from REELS spectra analysis: E_{pl} plasmon energy, n_{val} valence electron density, ρ calculated density, and Λ inelastic mean free path. $x(\%)$ is the relative nitrogen content with respect to carbon, as deduced by XPS data analysis (see text).

x (%)	E_{pl} (eV)	n_{val} (cm^{-3})	ρ (g cm^{-3})	Λ (nm)
0.0	26.9	5.25×10^{23}	2.614	3.25
10.4	25.7	4.79×10^{23}	2.367	3.56
25.0	24.0	4.18×10^{23}	2.047	4.09

The observed shift of the main plasmon towards lower energies finds its counterparts in the correspondent reduction of the density of valence electrons (-20.4%) and the mass density ρ of the samples (-21.7%). In particular, ρ has been evaluated as

$$\rho=\frac{n_{\mathrm{val}}(P_{\mathrm{C}}+P_{\mathrm{N}}x)}{N_a(N_{\mathrm{C}}+N_{\mathrm{N}}x)}, \tag{1}$$

where P_{C} and N_{C} (P_{N} and N_{N}) represent the atomic weight and the number of valence electrons for carbon (nitrogen) atoms, respectively, n_{val} is the valence electrons density and N_a is the Avogadro number. In Eq. (1) x is defined as the ratio [N]/[C] as deduced by the XPS 1s spectra of C and N.

Analyzing the behavior of $\mathrm{Im}(-1/\tilde{\epsilon})$ shown in Fig. 4, an energy variation is also observed in the case of π plasmons whose position ranges from 5.06 to 4.25 eV, the former energy being typical of the pure amorphous carbon.[26] As also observed by other authors,[19] π plasmon energy shifts at lower energies and its intensity is found to increase with increasing x. Both these two effects are to be ascribed to an increased threefold- to fourfold-coordination ratio. This is supported by the analysis of the complex N 1s XPS line which, as we have already pointed out, can be associated with an increase in the number of nitrogen atoms bonded to threefold- and fourfold-coordinated carbons. To simplify the analysis we can assume that the structure of a-CN_x films is essentially built up by only threefold- and fourfold-coordinated carbon atoms bonded to other carbon or nitrogen ones. These coordinations are generally identified in the literature as C-Csp^2, C-Csp^3, N-Csp^2, and N-Csp^3 bonds.[14,19,27] Thus, in order to justify the increase of the total threefold-coordination fraction, it should be necessary to hypothesize a decrease in the density of C-C fourfold coordination. Moreover, the shift to lower energies of the π plasmon is to be ascribed to the decrease of the sample densities that induce a reduction in the density of the involved π electrons. The two effects of the samples nitrogenation on the π plasmons, i.e., the increase of their intensity and the shift to lower energies, play a fundamental role in determining the threefold- to fourfold-coordination ratio. If, on one hand, the formation of threefold coordinations supplies new π electrons, on the other hand, it increases the average bond length in the structure reducing the mass density.[28] The overall spectral behavior is given by the balance between these two competing mechanisms.

As a consequence of the different features in the loss spectra also the REELS-deduced dielectric constant (Fig. 5) shows different spectral behaviors due to a modification of

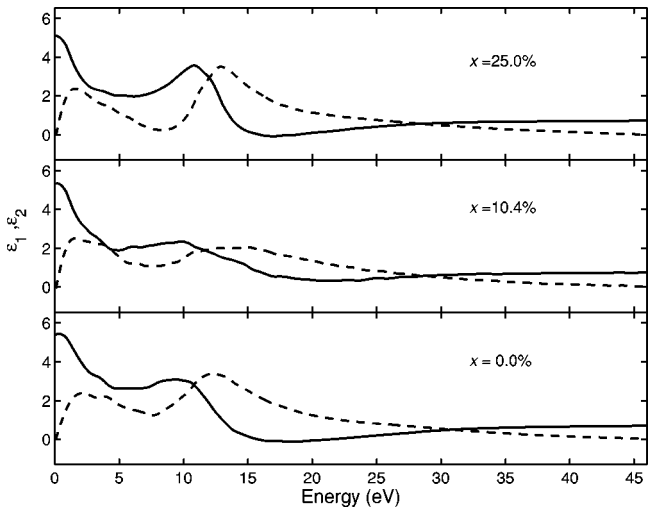

FIG. 5. Spectra of the real ϵ_1 (continuous line) and the imaginary ϵ_2 (dashed line) part of the dielectric constant deduced from Eqs. (A12) and (A13) for CN_x films having different nitrogen content (see Table I).

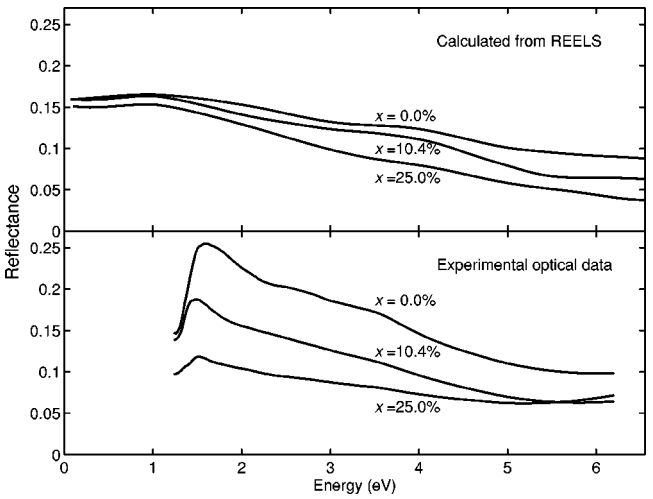

FIG. 6. Optical reflectivity spectra (lower) and REEL deduced ones (upper) for CN_x films having different nitrogen content (see Table I).

electronic levels with respect to the pure carbon band structure. It shows two separated groups of structures in ϵ_2 suggesting transitions that involve different groups of bands as in the case of graphite.[29] In that case, two spectral regions are defined below and above 8 eV, the first one dominated by intraband and interband transitions mainly of $\pi \rightarrow \pi^*$ character and the second by interband transitions of $\sigma \rightarrow \sigma^*$ character. A similar separation can be made for our samples of a-CN_x, being the two regions characterized by the same type of transitions. As can be observed in the behavior of the imaginary part of the dielectric constant, the higher nitrogen concentration gives a well-pronounced separation between the two groups of bands as in the case of graphite and this can be considered as a further proof of the nitrogen-induced graphitization of the material. Moreover, the structures in the left side of the low-energy region, centered at about 2.5 eV, show the tendency to increase their oscillator strength, this suggesting a reduction of the value of the energy gap and, possibly, an increase of the sample electrical conductivity. As pointed out in the Appendix, the loss function $\mathrm{Im}(-1/\tilde{\epsilon})$ has been normalized using a value of the dielectric constant at very low energy. Such a value has been deduced by the analysis of the interference fringes present in the near-infrared optical reflectivity of our samples. The results, in agreement with the decrease of the mass density upon nitrogenation, show a decrease of the index of refraction from 2.30 (pure amorphous carbon) to 2.20 for our higher nitrogen content. These values are some percent higher than those presented in Ref. 14, and this difference may be ascribed to the different sample preparation technique.

Finally, in Fig. 6, the reflectivity spectra of our samples are shown together with those measured by spectrophotometric methods. Taking into account the very different characteristics of the techniques adopted, the observed qualitative agreement is quite satisfactory. In particular, the spectra deduced by REELS in the optical limit and those obtained by optical spectroscopy essentially differ due to their very different energy resolutions. The optical functions provided by REEL spectroscopy, being a convolution of their natural line shape with a Gaussian response function that has the FWHM (1.4 eV) of the elastic peak, are more broadened and lowered than their spectrophotometric counterparts. The optical reflectivity data also show, upon increasing nitrogen content, a marked overall decrease compared to the EELS deduced ones. Since we found that the film surface roughness increases with the nitrogen content, an increased light scattering effect can be responsible for the substantial spread of our optical data. Nevertheless, from both the two sets of spectra is evident a continuous decrease of the reflectivity upon sample nitrogenation, with a contemporaneous shift towards low energies of the main structures. Thus, these results can also be interpreted on the basis of progressive reduction of the index of refraction, due to a lower mass density, induced by the increasing nitrogen concentration, accompanied with a graphitization of the material.

IV. CONCLUSION

In summary, the complex dielectric constant of CN_x films has been obtained in a very wide energy range (0–45 eV) by means of electron-energy-loss spectroscopy in the reflection mode. In particular, the results obtained can be summarized as follows.

From the point of view of the technique and of the methodology adopted, an appropriate choice of the approximations has allowed us to deconvolve the loss spectra and to extract, with a relatively simple procedure, the real and imaginary parts of the dielectric function. The use of the inelastically scattered electron spectroscopy offers the main advantage to provide optical spectra without problems arising from interference effects, at low frequencies, or light sources availability, at high frequencies, typical of the spectrophotometric techniques. The sensitivity of REELS in detecting small differences in the dielectric response has been confirmed by the good agreement with the optically determined reflectivity.

For what concerns the material properties, in the frame of our starting hypotheses on the nature of the bonds in CN_x, the nitrogen introduction in an amorphous carbon matrix has been found to induce an increase in the total threefold-

coordination fraction with a contemporaneous lowering of the C-C fourfold-coordination concentration. Then, as already observed by means of other diagnostic techniques,[19] there is clear evidence of a progressive graphitization of the material upon increasing the nitrogen content.

ACKNOWLEDGMENTS

This work was partially supported by the Italian National Research Council (CNR) through the ''Progetto Finalizzato Madess II.''

APPENDIX

The extracting procedure of the optical constants from the electron-energy-loss spectra is elsewhere described in details both for transmission (TEELS) and reflection (REELS) modes.[30–33] Here we report a more simple procedure for the extraction of the dielectric function from the loss data.

The analysis of a REEL spectrum is based on a simple phenomenological model in which the measured single scattering electron yield is represented by a linear combination of the bulk and surface loss functions

$$S(E)=k\{A\ \mathrm{Im}[-1/\tilde{\epsilon}]+B\ \mathrm{Im}[-1/(\tilde{\epsilon}+1)]\}, \qquad \text{(A1)}$$

where $\tilde{\epsilon}$ is the complex dielectric function and k is an instrumental scale constant. A and B are coefficients that mainly depend on the primary beam energy, its angle of incidence on the sample surface α, and the total mean free path Λ. In particular,

$$A=\int_d^{\infty}\exp\left(\frac{-2z}{\Lambda\cos\alpha}\right)dz=\frac{\Lambda\cos\alpha}{2}\exp\left(\frac{-2d}{\Lambda\cos\alpha}\right), \qquad \text{(A2)}$$

$$B=\int_0^{d}\exp\left(\frac{-2z}{\Lambda\cos\alpha}\right)dz=\frac{\Lambda\cos\alpha}{2}\left[1-\exp\left(\frac{-2d}{\Lambda\cos\alpha}\right)\right], \qquad \text{(A3)}$$

where z is a depth coordinate perpendicular to the sample surface and d is a phenomenological parameter which represents the thickness of that sample region where the surface scattering dominates. Its value is generally of the same order of magnitude of the wavelength of the impinging electrons.[34] In our case, for a primary energy of 2.5 keV, d is about 0.240 Å. When the ratio d/Λ decreases, the surface contribution to the measured yield decreases as well. Thus, samples characterized by large electron mean free paths show a spectrum which is mainly due to bulk effects. The value of Λ used for our REELS data analysis has been deduced by a universal function proposed for a wide variety of compounds.[35] Measuring the primary energy E_p in electronvolts and if M is the molecular weight in g/mol, N the number of valence electrons per structural unit (atom or molecule), and ρ the density in g/cm^3, the electron mean free path is given by

$$\Lambda(E_p)=\frac{ME_p}{\rho N(13.6\ln E_p-17.6-1400/E_p)}. \qquad \text{(A4)}$$

In order to proceed to the extraction of the optical functions from the raw data, the first step is the elimination of the elastic peak and the subtraction of the background (double scattering included). The former procedure is typically accomplished by a best fit of its Gaussian line shape. The latter is obtained by a self-consistent method suggested by Tougaard and Kraaer,[36,37]

$$F_lK(E_0-E)=\frac{1}{C}\left\{Y(E)-F_l\int_E^{E_0}K(E'-E)Y(E')dE'\right\} \qquad \text{(A5)}$$

with

$$F_l=\frac{\Lambda L}{\Lambda+L}, \qquad \text{(A6)}$$

where $K(E)$ is the background-free loss spectrum, $Y(E)$ the total experimental yield, L the attenuation length of the reflected electrons due to elastic scattering, and C the elastic peak area. Details concerning the application of this procedure can be elsewhere found.[38] A single scattering spectrum is thus obtained, built up by bulk and surface contributions where losses are due, typically in the first 30 eV, to interband transitions and plasmon excitations. In the second step, according to the standard procedures described in the literature, this single scattering spectrum shall be fitted to the model function for the REELS cross section and its yield subjected to the separation of surface and bulk terms.

In order to evaluate the relative weight of the A and B terms in Eq. (A1) it is necessary to estimate the total mean free path Λ, knowing N and ρ. In the free-electron approximation, the density n_{val} of valence electrons is given by the well-known Drude relation

$$n_{\mathrm{val}}=\frac{m}{4\pi e^2}E_{\mathrm{pl}}^2=7.25\times10^{20}E_{\mathrm{pl}}^2(\mathrm{eV}), \qquad \text{(A7)}$$

while the mass density ρ is given by

$$\rho=\frac{n_{\mathrm{val}}\sum\ (P_ix_i)}{N_a\sum\ (N_ix_i)}, \qquad \text{(A8)}$$

where E_{pl} is the main plasmon energy, m the electron mass, e the electron charge, N_a the Avogadro number, and $\Sigma(x_i)=1$. P_i, N_i, and x_i represent the atomic weight, the number of valence electrons, and the percentage fraction of the i atomic species, respectively. Strictly speaking, for a precise evaluation of the above quantities, it must be stressed that the eigenfrequencies of the bulk plasmons should be defined by the condition $\tilde{\epsilon}=0$ and not by the position of the plasmon peak. Moreover, when bound electrons are present, the dielectric constant and, consequently, the plasmon energies change with respect to those obtained by the simple Drude formula. However, such changes are not so drastic to invalidate the use of the free-electron approximation.[30] The Λ value is calculated from Eq. (A4), using the E_{pl} value obtained after the elimination of the elastic peak and the subtraction of the secondary electrons background. Such a choice may be justified by the fact that the surface counter-

part of the main plasmon lays at lower energies and has a minimal influence in determining the plasmon energy.

In the case of our samples, Λ values range from about 32 to 41 Å. Taking the ratio of the two coefficients B and A, defined by the Eqs. (A2) and (A3),

$$\frac{B}{A}=\exp\left(\frac{2d}{\Lambda\cos\alpha}\right)-1, \tag{A9}$$

we obtain, for our REEL spectra, a value slightly smaller than 3%. Consequently the surface contribution to the total single scattering yield is then negligible with respect to the bulk one. As a result, we have considered the background-free experimental spectra as essentially due to bulk scattering, i.e., directly proportional to $\mathrm{Im}(-1/\tilde{\epsilon})$.

A Kramers-Kronig transform is then used to deduce the real part of $-1/\tilde{\epsilon}$,

$$\mathrm{Re}\left(-\frac{1}{\tilde{\epsilon}(E)}\right)=1-\frac{2}{\pi}P\int_0^\infty c\,\mathrm{Im}\left(-\frac{1}{\tilde{\epsilon}(E')}\right)\frac{E'}{E'^2-E^2}dE'. \tag{A10}$$

For a semiconductor or an insulator the proportionality constant c is generally deduced knowing the value of the dielectric constant at very low energy, as deduced by optical reflectivity measurements,

$$c=\frac{\frac{\pi}{2}\left[1-\mathrm{Re}\left(-\frac{1}{\tilde{\epsilon}(0)}\right)\right]}{P\int_0^\infty\frac{\mathrm{Im}[-1/\tilde{\epsilon}(E')]}{E'}dE'}, \tag{A11}$$

where $\mathrm{Re}[-1/\tilde{\epsilon}(0)]$ is equal to $\epsilon_1^{-1}(0)$ being $\epsilon_2(0)=0$. 'Once known the real and imaginary parts of $-1/\tilde{\epsilon}$, the dielectric constant all over the experimental range is obtained by means of the following equations:

$$\epsilon_1=\frac{\mathrm{Re}\left(-\frac{1}{\tilde{\epsilon}}\right)}{\left[\mathrm{Re}\left(-\frac{1}{\tilde{\epsilon}}\right)\right]^2+\left[\mathrm{Im}\left(-\frac{1}{\tilde{\epsilon}}\right)\right]^2}, \tag{A12}$$

$$\epsilon_2=\frac{\mathrm{Im}\left(-\frac{1}{\tilde{\epsilon}}\right)}{\left[\mathrm{Re}\left(-\frac{1}{\tilde{\epsilon}}\right)\right]^2+\left[\mathrm{Im}\left(-\frac{1}{\tilde{\epsilon}}\right)\right]^2}. \tag{A13}$$

It has been shown[30] that, in the reflection mode, the maximum momentum transfer q upon collision of the primary electrons with the solid does not exceed 0.3 Å^{-1}. The dielectric constant deduced by the above procedure, taking into account the small momentum transfer of the impinging electrons (in our case about 0.102 Å^{-1} at an energy loss of 25 eV), is to be considered as substantially similar to that obtained by means of optical experiments. This assumption is usually referred to as the optical limit, i.e., when $\tilde{\epsilon}(E,q)=\tilde{\epsilon}(E)$.

*Email: mondio@ortica.unime.it

[1] A.Y. Liu and M.L. Cohen, Science **245**, 921 (1989).
[2] A.Y. Liu and M.L. Cohen, Phys. Rev. B **41**, 10 727 (1990).
[3] D.M. Teter and R.J. Hemley, Science **271**, 53 (1996).
[4] S.-D. Mo, L. Ouyang, W.Y. Ching, I. Tanaka, Y. Koyama, and R. Riedel, Phys. Rev. Lett. **83**, 5046 (1999).
[5] K.M. Yu, M.L. Cohen, E.E. Haller, W.L. Hansen, A.Y. Liu, and I.C. Wu, Phys. Rev. B **49**, 5034 (1994).
[6] Y. Guo and W.A. Goddard III, Chem. Phys. Lett. **237**, 72 (1995).
[7] A.Y. Liu and R.M. Wentzcovitch, Phys. Rev. B **50**, 10 362 (1994).
[8] S. Muhl, J.M. Mendez, Diamond Relat. Mater. **8**, 1809 (1999).
[9] Y.H. Yu, Z.Y. Chen, E.Z. Luo, W.Y. Cheung, J.P. Zhao, X. Wang, J.B. Xu, S.P. Wong, and I.H. Wilson, J. Appl. Phys. **87**, 2874 (2000).
[10] S.E. Rodil, N.A. Morrison, J. Robertson, and W.I. Milne, Phys. Status Solidi A **174**, 25 (1999).
[11] Y.F. Lu, Z.M. Ren, T.C. Chong, B.A. Cheong, S.I. Pang, J.P. Wang, and K. Li, J. Appl. Phys. **86**, 4954 (1999).
[12] K. Chakrabarti, M. Basu, S. Chaudhuri, A.K. Pal and H. Hanzawa, Vacuum **53**, 405 (1999).
[13] N. Tsubouchi, B. Enders, A.K. Chayahara, A. Kinomura, C. Heck, and Y. Horino, J. Vac. Sci. Technol. A **17**, 2384 (1999).
[14] S.R.P. Silva, J. Robertson, G.A.J. Amaratunga, B. Rafferty, L.M. Brown, J. Schwan, D.F. Franceschini, and G. Mariotto, J. Appl. Phys. **81**, 2626 (1997).
[15] N. Hellgren, M.P. Johansson, E. Broitman, L. Hultman, and J. Sundgren, Phys. Rev. B **59**, 5162 (1999).
[16] K. Yamamoto, Y. Koga, S. Fujiwara, F. Kokai, J. Kleiman, and K. Kim, Thin Solid Films **339**, 38 (1999).
[17] A. Mansour and D. Ugolini, Phys. Rev. B **47**, 10 201 (1993).
[18] S.R.P. Silva, R.U.A. Khan, A.P. Burden, J.V. Anguita, J.M. Shannon, B.J. Sealy, A.J. Papworth, C.J. Kiely, and G.A.J. Amaratunga, Thin Solid Films **332**, 118 (1998).
[19] S. Bhattacharyya, C. Valle, C. Cardinaud, O. Chauvet, and G. Turban, J. Appl. Phys. **85**, 2162 (1999).
[20] J. F. Moulder, W. F. Stickle, P. E. Sobol, and K. D. Bomben, in *Handbook of X-ray Photoelectron Spectroscopy*, edited by J. Chastain (Perkin-Elmer, Eden Prairie, 1992).
[21] C. Quiros, P. Prieto, A. Fernandez, E. Elizalde, C. Morant, R. Schlögl, O. Spillecke, and J.M. Sanz, J. Vac. Sci. Technol. A **18**, 515 (2000).
[22] J.M. Ripalda, E. Roman, N. Diaz, L. Galan, I. Montero, G. Comelli, A. Baraldi, S. Lizzit, A. Goldoni, and G. Paolucci, Phys. Rev. B **60**, R3705 (1999).
[23] N. Hellgren, M.P. Johansson, E. Broitman, L. Hultman, and J. Sundgren, Phys. Rev. B **59**, 5162 (1999).
[24] C. Ronning, H. Feldermann, R. Merk, H. Hofsäss, P. Reinke, and J.U. Thiele, Phys. Rev. B **58**, 2207 (1998).
[25] M.A. Baker and P. Hammer, Surf. Interface Anal. **25**, 301 (1997).
[26] G. Curro, G. Mondio, F. Neri, G. Compagnini, and G. Foti, J. Electron Spectrosc. Relat. Phenom. **72**, 89 (1995).
[27] F. Alvarez, M.C. dos Santos, and P. Hammer, Appl. Phys. Lett. **73**, 3521 (1998).

[28] J. Hu, P. Yang, and C.M. Lieber, Phys. Rev. B **57**, R3185 (1998).
[29] E.A. Taft and H.R. Philipp, Phys. Rev. A **138**, 197 (1965).
[30] H. Raether, in *Excitation of Plasmons and Interband Transitions by Electrons*, Springer Tracts in Modern Physics Vol. 88 (Springer-Verlag, Berlin, 1980).
[31] G. Mondio, F. Neri, G. Curró, S. Patané, and G. Compagnini, J. Mater. Res. **8**, 2627 (1993).
[32] G. Mondio, A.D. Laine, A.M. Mezzasalma, G. Cubiotti, and Yu.N. Kucherenko, J. Electron Spectrosc. Relat. Phenom. **85**, 1 (1997).
[33] G. Curró, F. Neri, G. Mondio, G. Compagnini, and G. Foti, Phys. Rev. B **49**, 8411 (1994).
[34] G. Chiarello, E. Colavita, M. De Crescenzi, and S. Nannarone, Phys. Rev. B **29**, 4878 (1984).
[35] E.T. Arakawa, M.W. Williams, J.C. Ashley, and L.R. Painter, J. Appl. Phys. **52**, 3579 (1981).
[36] S. Tougaard, J. Electron Spectrosc. Relat. Phenom. **52**, 243 (1990).
[37] S. Tougaard and J. Kraaer, Phys. Rev. B **43**, 1651 (1991).
[38] P. Prieto, F. Yubero, E. Elizalde, and J.M. Sanz, J. Vac. Sci. Technol. A **14**, 3181 (1996).